Structural Durability & Health Monitoring

Tech Science Press

https://doi.org/10.32604/sdhm.2026.080081

ARTICLE

Contact Friction Behavior Analysis of Spherical Hinges in Swing Bridges Using Finite Element and Meta-Modeling

Jiahao Wang[1], Yuanxun Zheng[1,*], Chaowei Du[1], Shuaijie Zhang[2], Xiangyang Chen[3], Xiaojun Che[4] and Fuhua Wang[5]

[1]School of Water Conservancy and Transportation, Zhengzhou University, Zhengzhou, China
[2]China Railway Taiyuan Group Co., Ltd., Taiyuan, China
[3]China Railway Seventh Bureau Group Zhengzhou Engineering Co., Ltd., Zhengzhou, China
[4]School of Transportation, Wuhan University of Technology, Wuhan, China
[5]CSSC Sunrui (Luoyang) Special Equipment Co., Ltd., Luoyang, China

*Corresponding Author: Yuanxun Zheng. Email: yxzheng@zzu.edu.cn

Received: 02 February 2026; Accepted: 29 April 2026; Published: 24 August 2026

ABSTRACT: Spherical hinges are critical load-bearing components in swing bridges, yet their complex contact friction behavior remains insufficiently investigated due to material and contact nonlinearities. Conventional parametric analysis based solely on finite element simulations suffers from low computational efficiency and limited consideration of multi-parameter coupling. In this study, a refined finite element model of an actual multi-lane swing bridge is established, and a support vector regression (SVR) metamodel is developed to efficiently predict contact stress distribution and frictional moments. Compared with existing studies that focus on single-factor parametric analysis, this work introduces a high-accuracy metamodel framework combined with global sensitivity analysis using Morris' basic effects method and Sobol' variance-based method. The SVR metamodel exhibits excellent predictive accuracy, with adjusted coefficients of determination exceeding 0.94 for all three characteristic indicators. Sensitivity analysis reveals that increasing the support radius significantly reduces maximum contact stress, while increasing swing weight linearly increases it; these two factors jointly dominate stress distribution. Additionally, decreasing curvature radius and increasing friction coefficient notably enhance horizontal and vertical frictional moments, with swing weight further amplifying these effects. The sensitivity rankings stabilize when the sample size exceeds 4000. This study provides an efficient and accurate metamodel-based framework for evaluating spherical hinge contact friction behavior, supporting design optimization and construction control of swing bridges.

KEYWORDS: Rotating bridges; ball-hinged structures; contact friction characteristics; meta-modeling; sensitivity analysis

1 Introduction

As a special construction technology, bridge transfer construction has been widely used in cross-line bridges, cross-canyon bridges and other projects by virtue of its advantages such as convenient construction and small interference with traffic. As the core force transmitting member of the transverse bridge, the contact friction characteristics of the spherical hinge directly affect the stability and structural safety of the transverse process. However, due to the complexity of the ball-hinge contact surface forces, which involves material nonlinearity, contact nonlinearity and friction effects, systematic research on its mechanical behavior remains lacking, which leads to the design relying on empirical formulas and potential risks. In particular, recent studies on nonlinear static analysis of simply supported prestressed concrete girder bridges considering shear deformation highlight the importance of refined mechanical modeling in bridge structural analysis [1]. Therefore, it is of great significance to construct an accurate ball-hinge contact friction proxy element model and analyze the sensitivity of key parameters to optimize the design and construction control of the transfer bridge.

In recent years, scholars at home and abroad have carried out certain researches on the mechanical properties of ball hinges of transverse bridges. In numerical simulation, the finite element method has been widely adopted in contact problems and parametric analysis. Parsons and Wilson [2] pioneered the application of the finite element analysis method to the structural mechanical analysis of two-dimensional elastic and frictionless contact problems in 1970; Chan and Tuba [3] used the finite element method to systematically analyze the two-dimensional and axisymmetric elastic contact problems with friction effect in 1971; Wang et al. [4] introduced the concept of virtual tribology, which employs modern technologies such as computer simulation and machine learning to study phenomena such as friction, wear, and lubrication, thereby advancing the use of numerical simulation methods to address contact friction problems; Liu et al. [5] used finite element analysis software to establish a refined finite element model of the ball hinge, and studied the effects of the radius of curvature, radius of the bearing and the arrangement of the ring rib on the mechanical properties of the ball hinge. He [6] studied the contact stress and force characteristics of the ball hinge, and proposed to take local strengthening of the ball hinge to ensure the safety of the construction of the rotating body; Sun and Hao [7] established a two-dimensional coordinated contact numerical model to analyze the stress distribution on the upper surface of the ball hinge through ANSYS; Huang et al. [8] used finite element analysis to investigate the structure of the rotating ball hinge, and then analyzed the impacts on the accuracy of the rotating hinge. The systematic numerical simulation of the rotating body ball-hinge structure was carried out to analyze the stress distribution characteristics and change rule of the ball-hinge contact region; Jiang and Gao [9] based on the finite element simulation method, systematically evaluated the influence degree of each error source on the solution accuracy of the contact problem and studied the distribution characteristics of the contact stresses; Fang [10] and Shi et al. [11] respectively, in the coordinated contact problem and the ball-hinge contact case without considering friction under the study. The finite element simulation method is applied, and the theoretical calculated values are compared with the finite element results, which shows that the accuracy of numerical simulation is better; Lan [12] investigates the relationship between the tonnage and radius of the ball hinge, and the distribution of the ball hinge stress is derived based on the finite element software, and a reasonable method is derived for solving the localized stress by comparing it with the theoretical values.

In summary, researchers have conducted numerical and experimental studies on spherical hinge behavior. Finite element methods have been widely used to analyze contact stress and parametric effects. However, existing studies predominantly focus on single-factor parametric analysis, lacking systematic exploration of multi-parameter coupling effects. Moreover, traditional finite element simulations are computationally expensive for large-scale parametric studies. To address these limitations, this study proposes a metamodel approach combined with global sensitivity analysis. A refined finite element model of a real-world multi-lane swing bridge is first established and validated. Then, a support vector regression (SVR)-based metamodel is constructed to efficiently predict key mechanical indicators. Morris and Sobol sensitivity analyses are employed to quantitatively evaluate the influence of seven key parameters. Compared with existing studies, this work offers a more efficient and comprehensive framework for evaluating spherical hinge contact friction behavior, supporting both design optimization and construction safety.

2 Dependent Projects

This study is based on a T-frame swing bridge crossing an existing railway line. The main girder is a 2 m × 80 m prestressed concrete box girder, with a total swing weight of 16,000 t (including guardrails and protection nets). The spherical hinge is the key load-bearing component during rotation. The upper turntable has a height of 2.5 m, and the lower turntable has a height of 4.0 m. The diameter of the spherical hinge for the rotating structure is 4.0 m. The layout of the rotating structure is shown in Fig. 1.

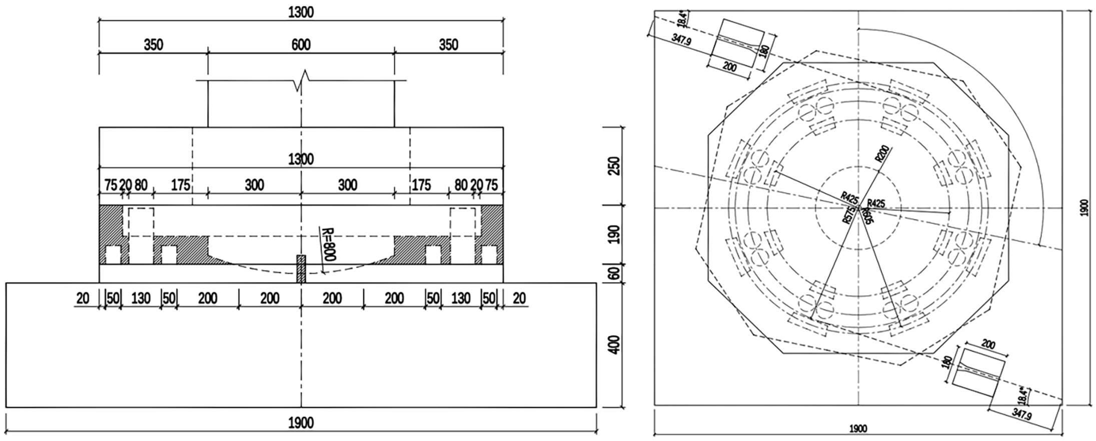

Figure 1: Rotating structure layout diagram.

3 Structural Finite Element Modeling

In this section, based on the right-span transverse bridge of the dependent project, ABAQUS software is used to establish the finite element numerical model of the transverse structure of the bridge [13], and the size of the model is the same as the actual engineering design, so as to ensure that the geometrical parameters of the components in the finite element analysis are fully matched with the real structure, which in turn accurately simulates the mechanical response of the structure and can take into consideration of the whole and the accurate simulation of the local mechanical behaviors.

The finite element numerical model of the rotor structure contains the upper turntable, turntable, upper ball hinge, lower ball hinge, lower turntable and other components, and each component is constructed according to the form and size of the actual structure, as shown in Fig. 2.

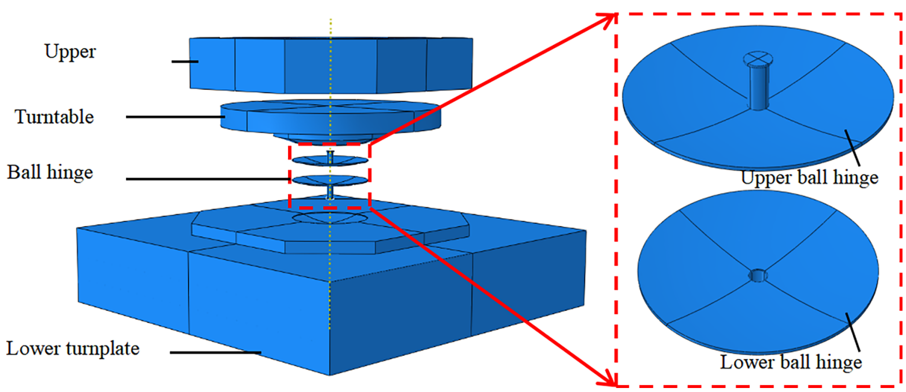

Figure 2: Component division of the finite element model of the rotor structure.

In this paper, the material setting is carried out according to the actual engineering design, the material of the upper and lower turntable and rotary table is set as C50 concrete, the material of the upper and lower ball-hinge structure is set as Q355D steel, the longitudinal and transverse prestressing tendons use ΦS15.2 strand, and the vertical prestressing tendons use Φ16-3 steel rods, and the specific parameters of the materials are shown in Table 1.

Table 1: Model material parameter values.

Part Name	Turntables, Rotary Tables	Ball Hinge	Longitudinal and Transverse Prestressing Tendons	Vertical Prestressing Tendons
Constituent material	C50 concrete	Q355D steel	ΦS15.2 steel stranded wire	Φ16-3 steel bar
Modulus of elasticity (MPa)	34,500	206,000	195,000	205,000
Poisson's ratio	0.20	0.28	0.30	0.30
Mass density (kg/m_3)	2420	7850	7850	7850
coefficient of friction	/	0.06	/	/
Expansion coefficient (1/°C)	/	/	1.2×10^{-5}	1.2×10^{-5}
Standard tensile strength (MPa)	/	/	1860	1420

The mesh type for each component was set to C3D8R reduced-order elements. This type of element significantly reduces computation time compared to full-order elements and performs well during mesh refinement. After meshing, the model had a total of 41,775 elements and 41,044 nodes. The mesh configuration for each component is shown in Fig. 3 and Table 2.

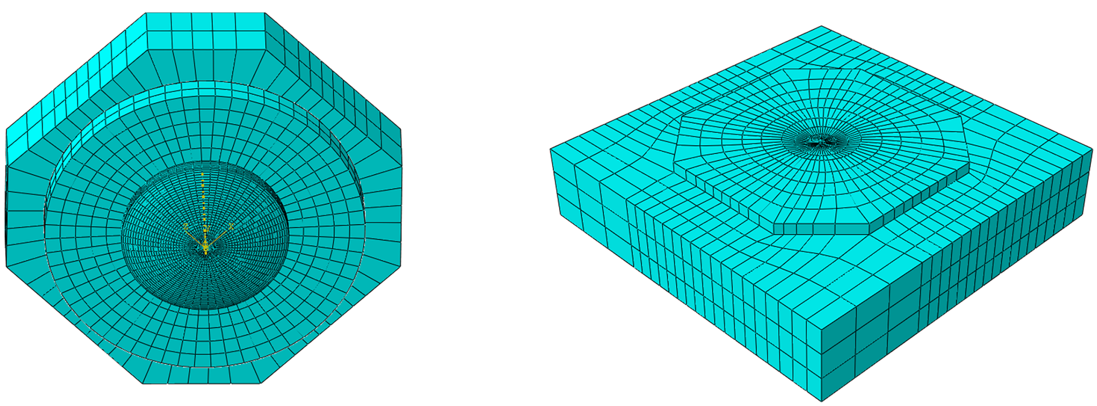

(a) **(b)**

Figure 3: (Continued)

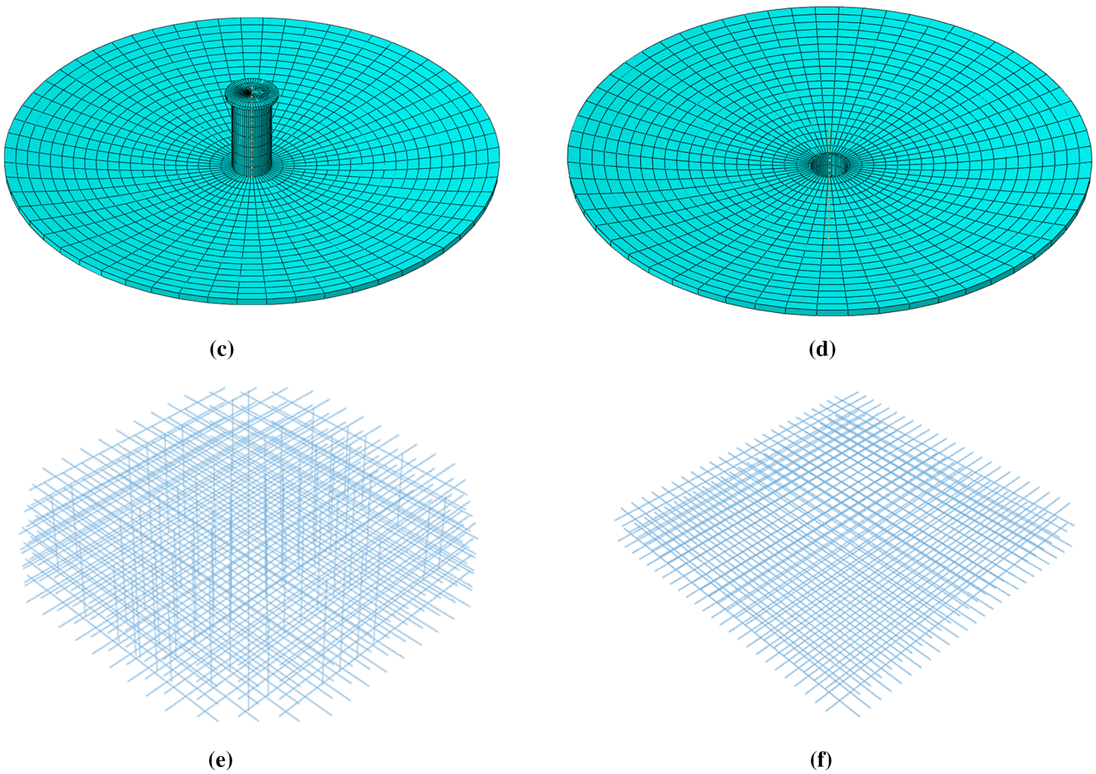

Figure 3: Mesh Division of Model Components. (**a**) Upper turntable and turntable; (**b**) Lower turntable; (**c**) Upper ball hinge; (**d**) Lower ball hinge; (**e**) Upper turntable prestressing tendons; (**f**) Lower turntable prestressing tendons.

Table 2: Components of a finite element model.

Component	Element Type	Element Count	Mesh Size (mm)
Upper/Lower turntable	C3D8R	12,845	50–80
Turntable	C3D8R	9234	50–80
Upper/Lower ball hinge	C3D8R	18,672	20–40
Prestressing tendons	T3D2	1024	100

Using the "Tie (binding)" function in the interaction of ABAQUS software to connect the upper turntable and the turntable of the rotating body structure in turn, and set the lower surface of the former as the master surface and the upper surface of the latter as the slave surface, and set the binding constraints of the two as shown in Fig. 4a.

Using the "Embedded" function in the software interaction, the upper ball hinge and the lower ball hinge are embedded in the rotary table and the lower turntable, in which the upper ball hinge and the rotary table are built-in constraints as an example, and the constraints of the two are shown in Fig. 4b.

A reference point (RP-1) was set at the center of the upper turntable and couple this reference point to the upper surface of the turntable. The weight of the main bridge's rotating section is 16,000 t. As the load for this model, apply the load (F = -1.6×10^8 N) as a concentrated force at this reference point (RP-1). The load was applied uniformly at a constant rate over a single analysis step of 1 s.

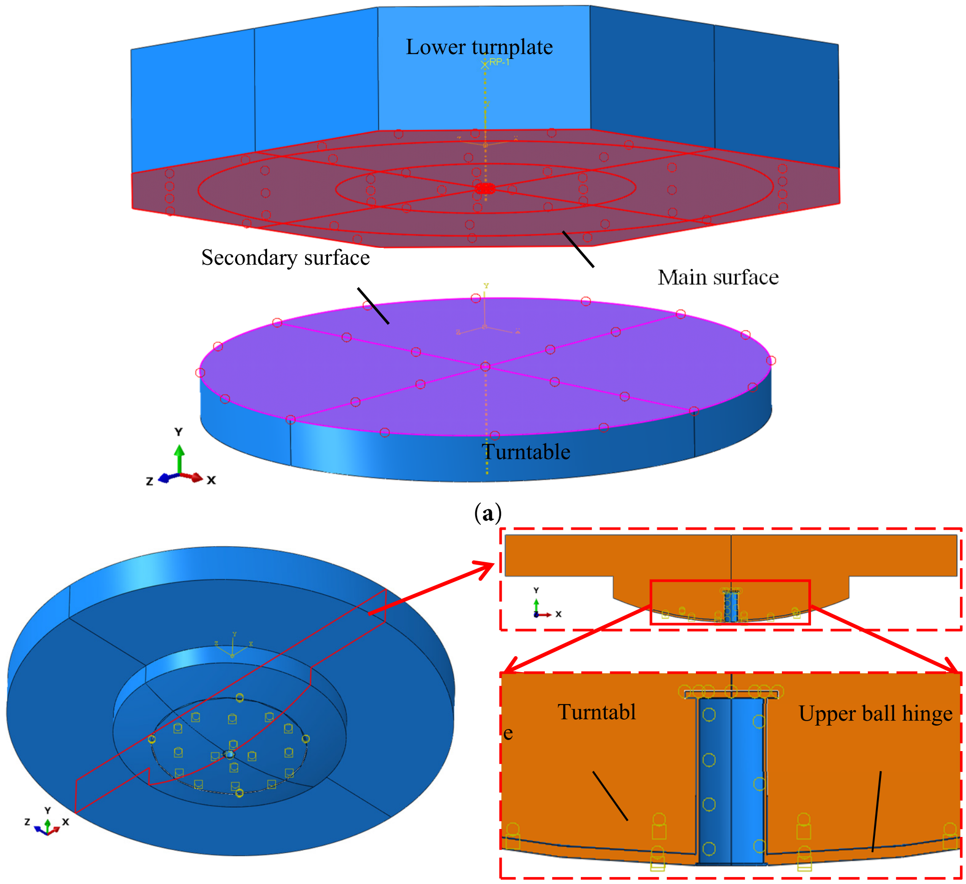

(**a**)

(**b**)

Figure 4: Constraints between the upper turntable, the upper ball hinge, and the turntable. (**a**) Binding constraints of the upper turntable to the turntable; (**b**) Constraints between the upper turntable, the upper ball hinge, and the turntable.

4 Metamodel of Force Characteristics of Rotating Ball Hinge

Although finite element analysis provides high-fidelity predictions of spherical hinge behavior, conducting parametric studies with a large number of input variables and their combinations becomes computationally expensive. To overcome this limitation, a metamodel approach is introduced. The metamodel serves as a computationally efficient approximation of the FE model, enabling rapid prediction of mechanical responses under varying input parameters. This allows for extensive parametric sensitivity analysis and supports design optimization with significantly reduced computational cost, while maintaining acceptable accuracy.

In this section, the simulation data on the contact stress values at the ball-hinge interface in the previous sections are extracted, and accordingly, the relationship between the spherical hinge contact stress and the distance from the center of the ball-hinge is plotted, as shown in Fig. 5.

By fitting a polynomial to the ball-hinge contact stress and the distance from the center of the ball-hinge, it was found that there is a significant correlation between the two, which is in good agreement with the results of the quadratic and cubic term fits in the existing research literature [14].

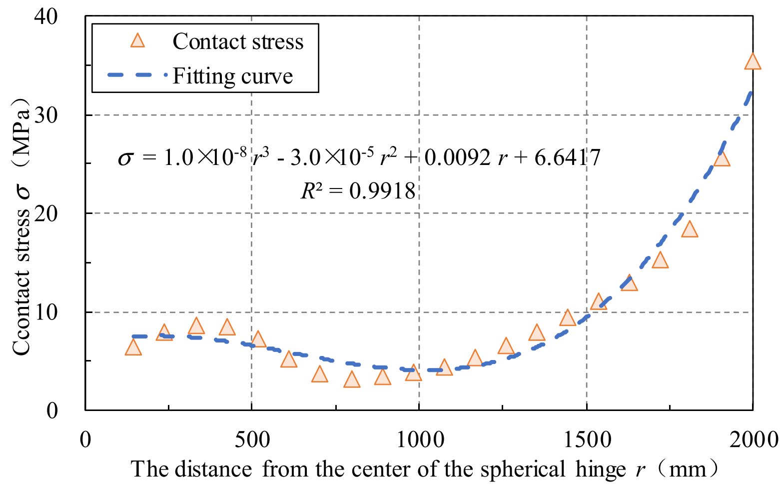

Figure 5: Curve of ball-hinge contact stress σ vs. distance r from ball-hinge center.

A cubic polynomial provides a better fit for the data in this study because the stress concentration phenomenon at the center pin is taken into account, and the correlation coefficient R2 can reach more than 0.99. The fitting equation can be uniformly expressed as:

$$\sigma = Ar^3 + Br^2 + Cr + D \tag{1}$$

In the above equation, σ denotes the ball-hinge contact stress; r denotes the distance of the stress point from the center of the ball-hinge; A, B, C and D are the fitting coefficients, respectively. A complete list of symbols and their descriptions is provided in Appendix A.

In this study, the maximum contact stress, vertical drag moment and horizontal drag moment of the ball hinge were selected as the characteristic indexes of the ball hinge contact friction force characteristics.

In a rotating structure, the contact friction force characteristics of the ball hinge are crucial to ensure the stability, safety and functionality of the structure. In-depth analysis of the influence of key factors on the contact friction force characteristics of ball hinges can provide theoretical support and practical guidance for optimizing structural design, improving structural reliability and extending structural service life. The main influencing factors on the ball-hinge contact friction force characteristics of the rotary bridge include the ball-hinge size parameters, ball-hinge material parameters and load factors.

4.1 Selection of Metamodel

When solving nonlinear complex problems in engineering structures, metamodels are usually established to simulate the mapping relationship between input and output parameters [15,16], and the commonly used metamodels include polynomial chaos expansion, artificial neural network, Gaussian process regression, radial basis function, support vector machine, etc. [17], and the performances of these models are largely affected by the computation time, simulation accuracy, quality of the input parameters and the number of samples. In this study, the polynomial chaos expansion (PCE), Gaussian process regression (Kriging) and support vector regression (SVR) are selected to construct the metamodel after considering the actual engineering background and the efficiency and robustness of the model [18].

(1) Polynomial Chaos Expansion (PCE)

The basic principle of Polynomial Chaos Expansion (PCE) is to represent the output response of a stochastic system driven by an N-dimensional random input variable by a set of orthogonal polynomial expansions modeled with respect to the variable x in the general form:

$$\mathrm{M}_{PCE}\left(\boldsymbol{x}\right) = \sum_{i=0}^{\infty} \beta_i \Theta_i\left(\boldsymbol{x}\right) \tag{2}$$

In the above equation, $\mathrm{M}_{PCE}\left(\boldsymbol{x}\right)$ is the model output corresponding to the input variable $\boldsymbol{x}$; $\Theta_i\left(\boldsymbol{x}\right)$ is the orthogonal polynomial basis function; β_i is the coefficient corresponding to the basis function.

(2) Gaussian process regression (Kriging)

Gaussian process regression (Kriging) is an unbiased estimation model for the analysis of complex nonlinear problems, and the general form of this model is [19]:

$$M_K\left(\boldsymbol{x}\right) = \boldsymbol{\beta}^T f\left(\boldsymbol{x}\right) + \sigma^2 Z\left(\boldsymbol{x}, \omega\right) \tag{3}$$

In the above equation, $\boldsymbol{x}$ is the model input parameter; $M_K\left(\boldsymbol{x}\right)$ is the model output for the input parameter $\boldsymbol{x}$; $\boldsymbol{\beta}^T f\left(\boldsymbol{x}\right)$ is the trend function, which is the mean value of the Gaussian process regression, and consists of a vector of basis functions, $f\left(\boldsymbol{x}\right)$, and a vector of regression coefficients, $\boldsymbol{\beta}$; and σ^2 and ω are the model variance and probability space, respectively.

The selection of the kernel function has a large impact on the final performance of the high-dimensional feature space structure and model, therefore, in the actual application should be based on their own needs in order to select the appropriate kernel function, the common kernel function is mainly a linear kernel function, polynomial kernel function, Sigmoid kernel function, and radial basis kernel function and so on.

The Radial Basis Function (RBF) kernel function, also known as the Gaussian kernel function, is a commonly used kernel function in machine learning. The kernel function has a high learning capacity and it contains only one width variable, which is suitable for any distribution and is perfectly suited for structural reliability calculations. Especially in support vector machines and Gaussian process regression. The RBF kernel function works by measuring the similarity between sample points in the following mathematical form:

$$k\left(x_i, x_j\right) = \exp\left(-\frac{\left\|x_i - x_j\right\|^2}{2\sigma^2}\right) \tag{4}$$

In the above equation, $\left\|x_i - x_j\right\|^2$ is the square of the Euclidean distance between points x_i and x_j; σ is a length scale parameter that controls the smoothness of the function.

(3) Support Vector Regression (SVR)

Support Vector Regression (SVR) is an application of Support Vector Machines (SVMs) [20] to regression analysis problems, which, for nonlinear problems, are of the general form:

$$M_{SVM}\left(\boldsymbol{x}\right) = \sum_{j=1}^{N} \left(\alpha_i - \alpha_i^*\right) k\left(\boldsymbol{x_i}, \boldsymbol{x}\right) + b \tag{5}$$

In the above equation, α_i and $\alpha_i{}^*$ are the Lagrange multipliers; $k\left(x_i, x\right)$ is the kernel function (using the Matérn kernel function).

4.2 Data Sets for Metamodeling

In view of the infeasibility of the actual test and the high efficiency and economic advantages of the finite element simulation, coupled with the fact that the numerical model established in this study has been verified to be accurate and effective, the current choice of finite element simulation is the optimal solution. Therefore, this study combines the practical situation, using the finite element model calculation to generate high-quality data to build a basic database, which can provide effective data support for the establishment of the metamodel, and then make the model have excellent generalization ability.

In order to investigate the influence of various factors on the contact friction force characteristics of the ball hinge, synthesizing the existing research status and the index system discussed in the previous section, this paper selects the radius of curvature of the ball hinge, support radius, pin radius, modulus of elasticity, Poisson's ratio, friction coefficient and the weight of the rotating body to construct a model of the input indexes, and carry out the relevant research.

In this study, the ball-hinge related parameters in the aforementioned engineering examples are used as the benchmark value, and the number of factors at a certain level of hierarchy is selected within a certain range of the benchmark value. In this study, the weight of bridge transitions in the project example is 16,000 t. Five levels of 14,000, 15,000, 16,000, 17,000 and 18,000 t are selected as the level levels of the factor of transition weight. The above seven input indicators are divided into level tiers, as shown in Table 3.

Table 3: Breakdown of input indicators by level hierarchy.

Indicator Name	Reference Value	Tier 1	Tier 2	Tier 3	Tier IV	Tier 5
Radius of curvature (mm)	8000	8000	9000	10,000	/	/
Support radius (mm)	2000	2000	2100	2200	/	/
Pin radius (mm)	146.5	100	200	300	/	/
Modulus of elasticity (MPa)	206,000	202,000	204,000	206,000	208,000	210,000
Poisson's ratio	0.28	0.26	0.27	0.28	0.29	0.30
coefficient of friction	0.06	0.03	0.04	0.05	0.06	0.07
Turning weight (N)	1.6 × 108	1.4 × 108	1.5 × 108	1.6 × 108	1.7 × 108	1.8 × 108

Based on ABAQUS finite element software, three levels of three factors, namely radius of curvature, radius of support and radius of pin, are combined to obtain 3ˆ3 = 27 kinds of basic working conditions, as shown in Table 4, and the finite element models of these 27 kinds of basic working conditions are constructed, and then exported to generate the 27 sets of inp files. And then according to the principle of orthogonal test design, five layers of four factors, namely, modulus of elasticity, Poisson's ratio, friction coefficient and weight of the rotating body, are combined and designed to construct the L25 (54) orthogonal test scheme, and 25 groups of parametric working conditions are obtained, as shown in Table 5.

Table 4: Numerical model base conditions (in mm).

Serial Number	Working Condition Serial Number	Curvature Radius	Support Radius	Pin Radius	Serial Number	Working Condition Serial Number	Curvature Radius	Support Radius	Pin Radius
1	8-20-1	8000	2000	100	15	9-21-3	9000	2100	300
2	8-20-2	8000	2000	200	16	9-22-1	9000	2200	100
3	8-20-3	8000	2000	300	17	9-22-2	9000	2200	200

(Continued)

Table 4 (continued)

Serial Number	Working Condition Serial Number	Curvature Radius	Support Radius	Pin Radius	Serial Number	Working Condition Serial Number	Curvature Radius	Support Radius	Pin Radius
4	8-21-1	8000	2100	100	18	9-22-3	9000	2200	300
5	8-21-2	8000	2100	200	19	10-20-1	10,000	2000	100
6	8-21-3	8000	2100	300	20	10-20-2	10,000	2000	200
7	8-22-1	8000	2200	100	21	10-20-3	10,000	2000	300
8	8-22-2	8000	2200	200	22	10-21-1	10,000	2100	100
9	8-22-3	8000	2200	300	23	10-21-2	10,000	2100	200
10	9-20-1	9000	2000	100	24	10-21-3	10,000	2100	300
11	9-20-2	9000	2000	200	25	10-22-1	10,000	2200	100
12	9-20-3	9000	2000	300	26	10-22-2	10,000	2200	200
13	9-21-1	9000	2100	100	27	10-22-3	10,000	2200	300
14	9-21-2	9000	2100	200	/	/	/	/	/

Table 5: L(25) (54) orthogonal test program.

Serial Number	Modulus of Elasticity (MPa)	Turning Weight (kN)	Coefficient of Friction	Poisson's Ratio	Serial Number	Modulus of Elasticity (MPa)	Turning Weight (kN)	Coefficient of Friction	Poisson's Ratio
1	202,000	140,000	0.03	0.26	14	208,000	180,000	0.03	0.27
2	204,000	160,000	0.06	0.30	15	210,000	150,000	0.06	0.26
3	206,000	180,000	0.04	0.29	16	202,000	160,000	0.07	0.27
4	208,000	150,000	0.07	0.28	17	204,000	180,000	0.05	0.26
5	210,000	170,000	0.05	0.27	18	206,000	150,000	0.03	0.30
6	202,000	180,000	0.06	0.28	19	208,000	170,000	0.06	0.29
7	204,000	150,000	0.04	0.27	20	210,000	140,000	0.04	0.28
8	206,000	170,000	0.07	0.26	21	202,000	150,000	0.05	0.29
9	208,000	140,000	0.05	0.30	22	204,000	170,000	0.03	0.28
10	210,000	160,000	0.03	0.29	23	206,000	140,000	0.06	0.27
11	202,000	170,000	0.04	0.30	24	208,000	160,000	0.04	0.26
12	204,000	140,000	0.07	0.29	25	210,000	180,000	0.07	0.30
13	206,000	160,000	0.05	0.28	/	/	/	/	/

Combining 27 basic working conditions and 25 groups of parameter working conditions, we get 27 × 25 = 675 groups of working conditions, and then we use Python to carry out secondary development to get the inp calculation file and bat execution file of 675 groups of working conditions in batch. Then run the bat file in batch to get the odb file of the calculation results, and write the data batch extraction code to get the final result data, i.e., the database required for this study. The calculation flow of ABAQUS and Python secondary development of the working conditions is shown in Fig. 6.

In this paper, the finite element software is used to simulate and calculate 675 sets of working conditions, which are set up by considering 7 input indicators and 3 output indicators, which are the key parameters affecting the force characteristics of the ball-hinge contact surface and the indicators characterizing the force characteristics. The constructed metrics for metamodel fitting are shown in Table 6.

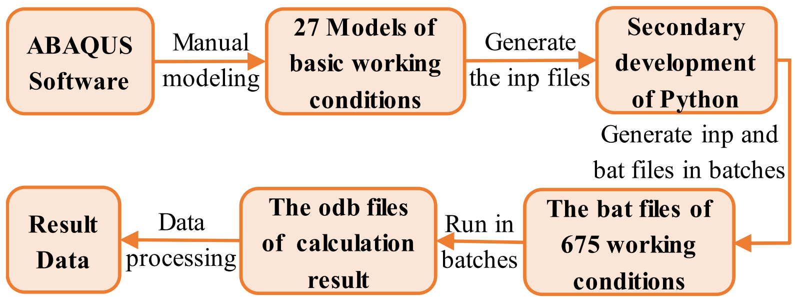

Figure 6: ABAQUS and Python secondary development of work condition calculation flow.

Table 6: Indicator system for force characterization of ball-hinged contact surfaces.

Type of Indicator	Serial Number	Indicator Name	Unit (of Measure)	Distributional Characteristics	Reference Value	Interval (Math.)
Input indicators (impact factors)	X1	Curvature radius	mm	U	8000	[8000, 10,000]
	X2	Support radius	mm	U	2000	[2000, 2200]
	X3	Pin radius	mm	U	146.5	[100, 300]
	X4	modulus of elasticity	MPa	U	206,000	[202,000, 210,000]
	X5	Poisson's ratio	/	U	0.28	[0.26, 0.30]
	X6	coefficient of friction	/	U	0.06	[0.03, 0.07]
	X7	rotary weight	kN	U	1.6 × 105	[1.4 × 105, 1.8 × 105]
Output metrics (Characterization indicators)	S1	Maximum contact stress	MPa	LN	30.17	(20, 50)
	S2	Horizontal Moment of Resistance	kN-m	LN	11,354.46	(0, 40,000)
	S3	Vertical moment of resistance	kN-m	LN	34,675.40	(0, 80,000)

Note: U denotes uniform distribution and LN denotes lognormal distribution. Output indicator distribution intervals are estimated rounding intervals.

In this study, each input and output index parameter has a clear physical or geometric meaning, and the respective variables are divided into level hierarchies with the same intervals during the design of the working conditions, so that the input indexes are uniformly distributed. For the output indicators, Fig. 7 shows the frequency distribution and cumulative probability of each output indicator, and the probability distribution characteristics are fitted using normal and lognormal distributions, respectively, and the fitted effects are obtained as shown in Table 7, and it can be found that the logarithmic adjusted R2 of the three output indicators is larger than the adjusted R2, so the three output variables are more suitable to be fitted by the log-normal distribution, and the output sets will be subsequently generated based on the best-fit distributions.

4.3 Metamodel Fitting Establishment

In order to further eliminate scale differences in the data of the variables in the indicator system, increase the generalization ability of the metamodel, and accelerate the convergence speed of the model, the data need to be normalized. For the input indicators, they are normalized because they are uniformly distributed; for the output indicators, they are usually standardized because they are (logarithmically) normally distributed. The probability distributions of the sample values of the input indicators X1~X7 after normalization are shown in Fig. 8, which all conform to the uniform distribution U(0, 1). The probability distributions of the sample values of the output indicators S1~S3 after normalization are shown in Fig. 9, which all conform to the standard normal distribution N(0, 1).

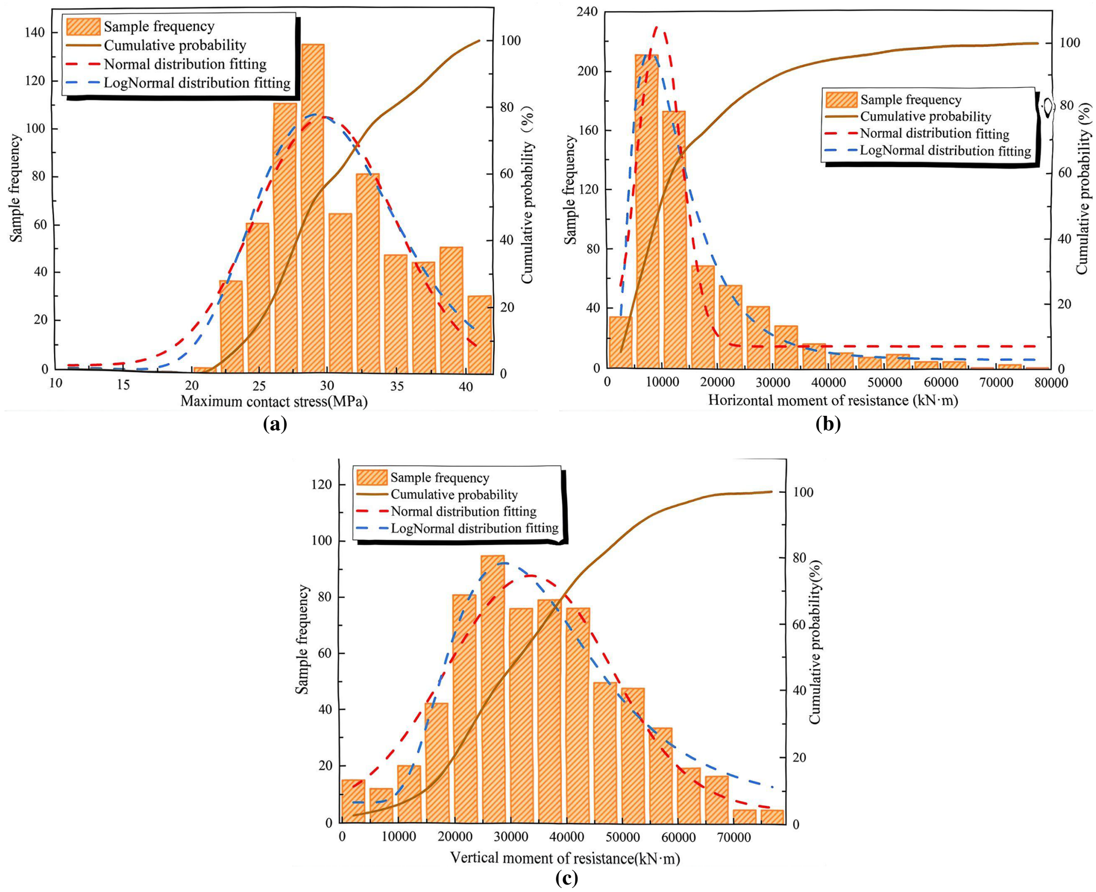

Figure 7: Frequency distribution characteristics and cumulative probability of output metrics. (**a**) S1 (Maximum contact stress); (**b**) S2 (Horizontal moment of resistance); (**c**) S3 (Vertical moment of resistance).

Table 7: Results of fitting the probability distribution characteristics of the output metrics.

Output Metrics	**Maximum Contact Stress**	**Horizontal Moment of Resistance**	**Vertical Moment of Resistance**
Adjustment R2	0.86041	0.90209	0.91806
Logarithmic adjustment R2	0.92823	0.97726	0.94407
Mean	29.86148	9805.49721	33,564.82335
Logarithmic Mean LN Mean	30.17633	11,354.45688	34,675.39644
Standard deviation SD	0.67402	419.04105	970.35677
Log standard deviation LN SD	0.61315	417.07151	1229.59769

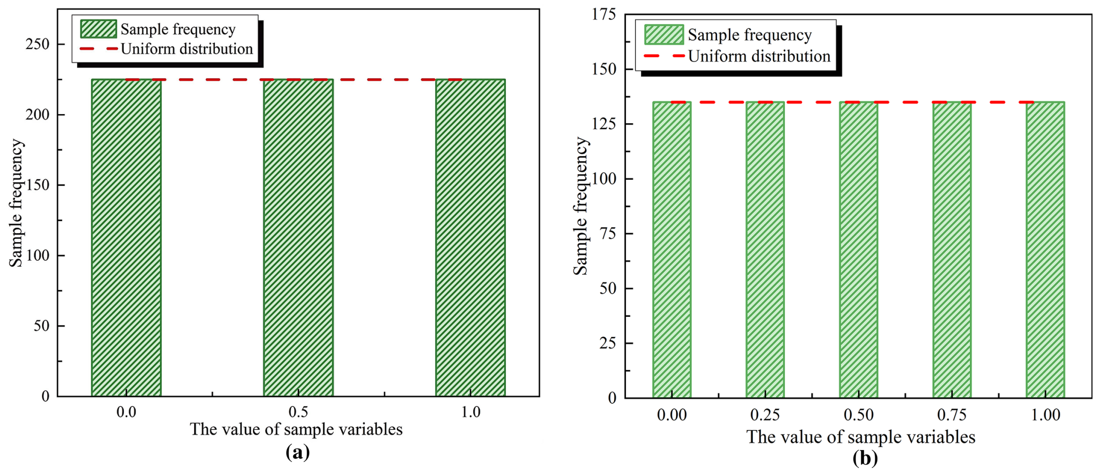

Figure 8: Frequency distribution characteristics of input metrics. (**a**) Input indicators X1 to X3; (**b**) Input indicators X4 to X7.

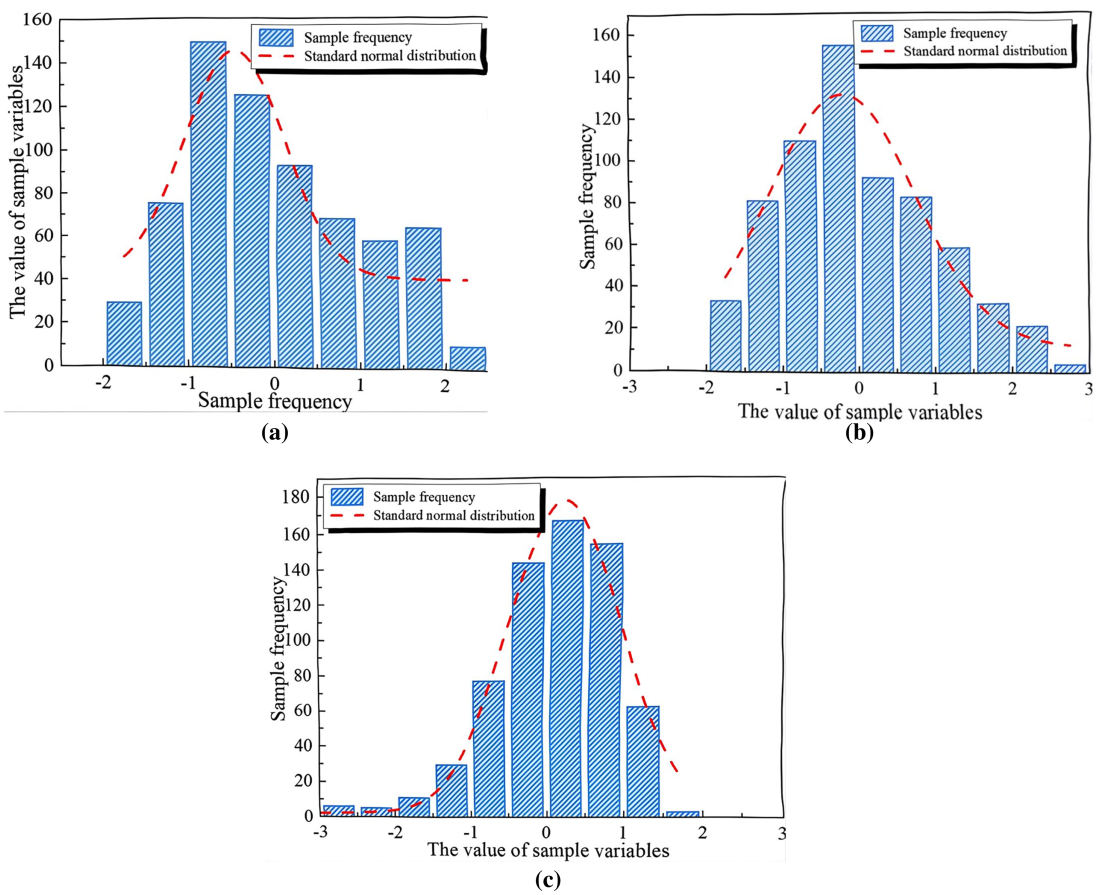

Figure 9: Frequency distribution characteristics of output indicators. (**a**) S1 (Maximum contact stress); (**b**) S2 (Horizontal moment of resistance); (**c**) S3 (Vertical moment of resistance).

In this paper, the metamodel is constructed relying on the above processed metrics as the dataset, but since the input and output parameters in finite element analysis are nonlinear and strongly coupled, the accuracy of the metamodel constructed by using a limited number of sample points is always limited, or the mapping relationship between the data can not be fully explained to some extent. Therefore, the root mean square error (RMSE), the mean absolute error (MAE), the coefficient of determination (R2) and R2adjusted are used as the evaluation indexes to verify the precision and accuracy of the constructed metamodels [21]. The formulas of R2 and R2adjusted are as follows:

$$R^2 = 1 - \frac{\sum_{i=1}^{n} \left(y_i - y_i^*\right)^2}{\sum_{i=1}^{n} \left(y_i - \overline{y}\right)^2} \tag{6}$$

$$R^2_{adjusted} = 1 - \frac{n-1}{n-p-1} \times \left(1 - R^2\right) \tag{7}$$

In the above equation, p denotes the number of independent variables; n denotes the number of samples; y_i denotes the true value of the data; y_i* denotes the predicted value of the data; and $\overline{y}$ denotes the average value of the data. If the value of R^2 and $R^2{}_{adjusted}$ is closer to 1, it indicates that the metamodel is more capable of explaining the data and its fitting effect is better.

In order to improve the model performance, this study performed parameter tuning based on the GridSearchCV tool provided in Scikit-learn, a software machine learning library for Python. The best combination of parameters was found by traversing the given parameter grid using 5-fold cross-validation (5-CV) and the model was further trained using these parameters.

Since the accuracy of the metamodel is greatly affected by its type and the number of samples in the dataset, machine learning metamodels with output (feature) metrics S1~S3 are constructed in this paper by using three methods: PCE, Kriging, and SVR, respectively. In order to comprehensively evaluate the performance of the metamodel, the 675 sets of data in this paper are divided into nine sample sets of 75, 150, 225, 300, 375, 450, 525, 600, and 675 for the training and testing of the metamodel.

In order to obtain more reliable and reasonable results, and to find the optimal sample set and the optimal metamodel, this study resampled each sample set 50 times, summarized the R2 adjusted values of different metamodels in the case of 50 samples in order to evaluate their fitting effects, and plotted the optimized parameters corresponding to the optimized metamodels for each output (feature) metrics (hereinafter referred to as feature metrics). The box plots of the fitting effect are shown in Fig. 10.

From Fig. 10, it can be found that the fit of the metamodel constructed using SVR is better than that of PCE and Kriging metamodel. For the feature metrics S1~S3, the mean value of R(2) (adjusted) of SVR metamodel under 50 times of re-sampling reaches the maximum at the sample numbers of 450, 450, and 600, which can be up to 0.9593, 0.9557, and 0.9429, respectively. times of 525, 450, and 600 can be up to 0.9941, 0.9925, and 0.9967, respectively, demonstrating excellent fitting ability. In contrast, the metamodel established by PCE and Kriging is worse than the SVR metamodel in terms of fitting effect. For the feature indicators S1~S3, the mean values of R2adjusted fluctuate within the ranges of 0.80~0.95, 0.80~0.90, and 0.70~0.90, respectively, for the 50 repetitions of samples, but the values of R2(adjusted) gradually converge with the increase of the number of samples, and the values of R2(adjusted) gradually converge to 0.9941, 0.9925, and 0.9967, respectively, with the increase of the number of samples. values gradually leveled off as the number of samples increased and eventually floated around 0.90, but failed to reach the fitting level of the SVR metamodel.

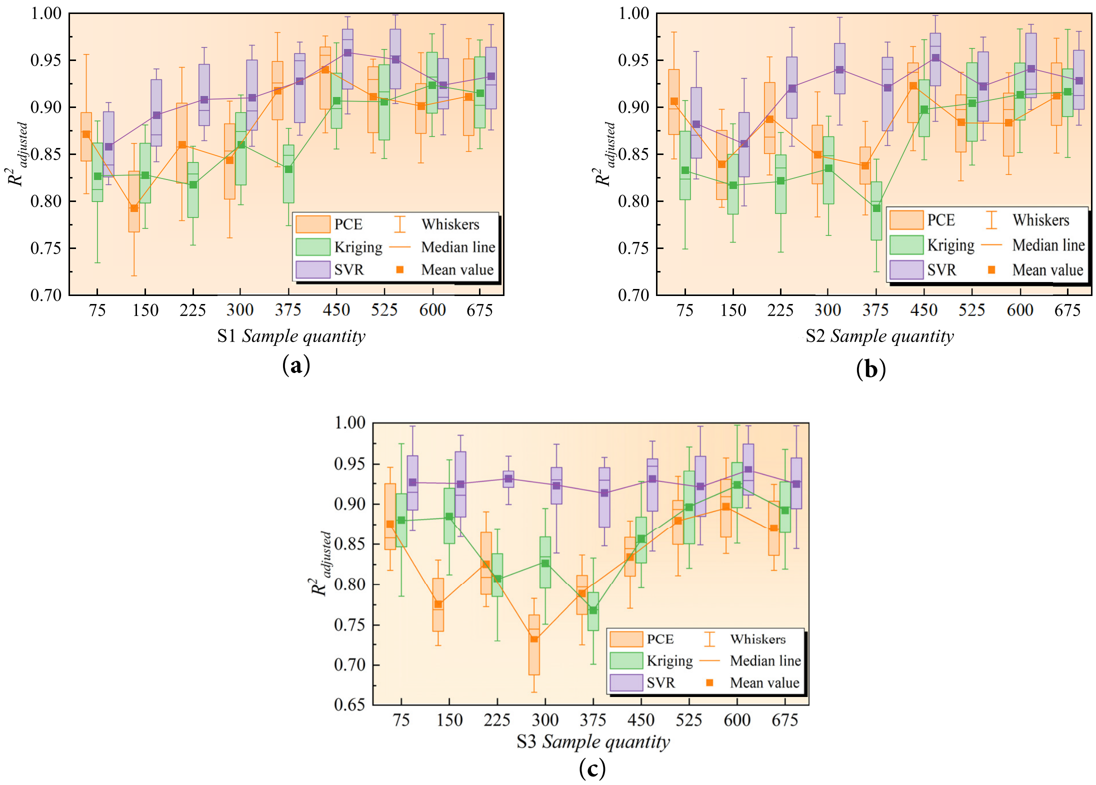

Figure 10: Box plots of the distribution of the effects of the 10-element model fit. (**a**) Output indicator S1; (**b**) Output indicator S2; (**c**) Output indicator S3.

When the sample size is in the range of 500–700, the SVR metamodel shows the best generalization ability and fitting effect. The results of the training and testing of the three feature metrics using the SVR metamodel are shown in Fig. 11. The figure shows the fitting of all 675 sets of data for each of the three feature metrics, of which 473 sets of data (70%) are the training set.

In this study, the SVR method was finally adopted to construct a metamodel for the force characteristics of the ball-hinge contact surface. This choice is not only based on the excellent performance of the SVR metamodel in terms of fitting effect and generalization ability, but also takes into full consideration of the characteristics of the sample data and research needs. Through this method, the force characteristics of the ball-hinge contact surfaces can be predicted and evaluated more accurately, which can provide a strong support for the research in related fields.

As shown in Fig. 11a–c, for the three feature indicators from S1 to S3, the real values of the training set of the SVR metamodel are in agreement with the predicted values, and the R^2 values can reach 0.9583, 0.9621 and 0.9378, respectively, and the model exhibits an excellent fitting effect in the training stage.

In summary, the generalization ability of the SVR metamodel for the three feature indicators from S1 to S3 is better for the training set, and the prediction results are consistent with the actual values, and the R^2 values are kept above 0.93, which fully demonstrates the good prediction effect and robustness of the model. This also provides a strong theoretical support for the use of SVR model for relevant prediction in practical applications.

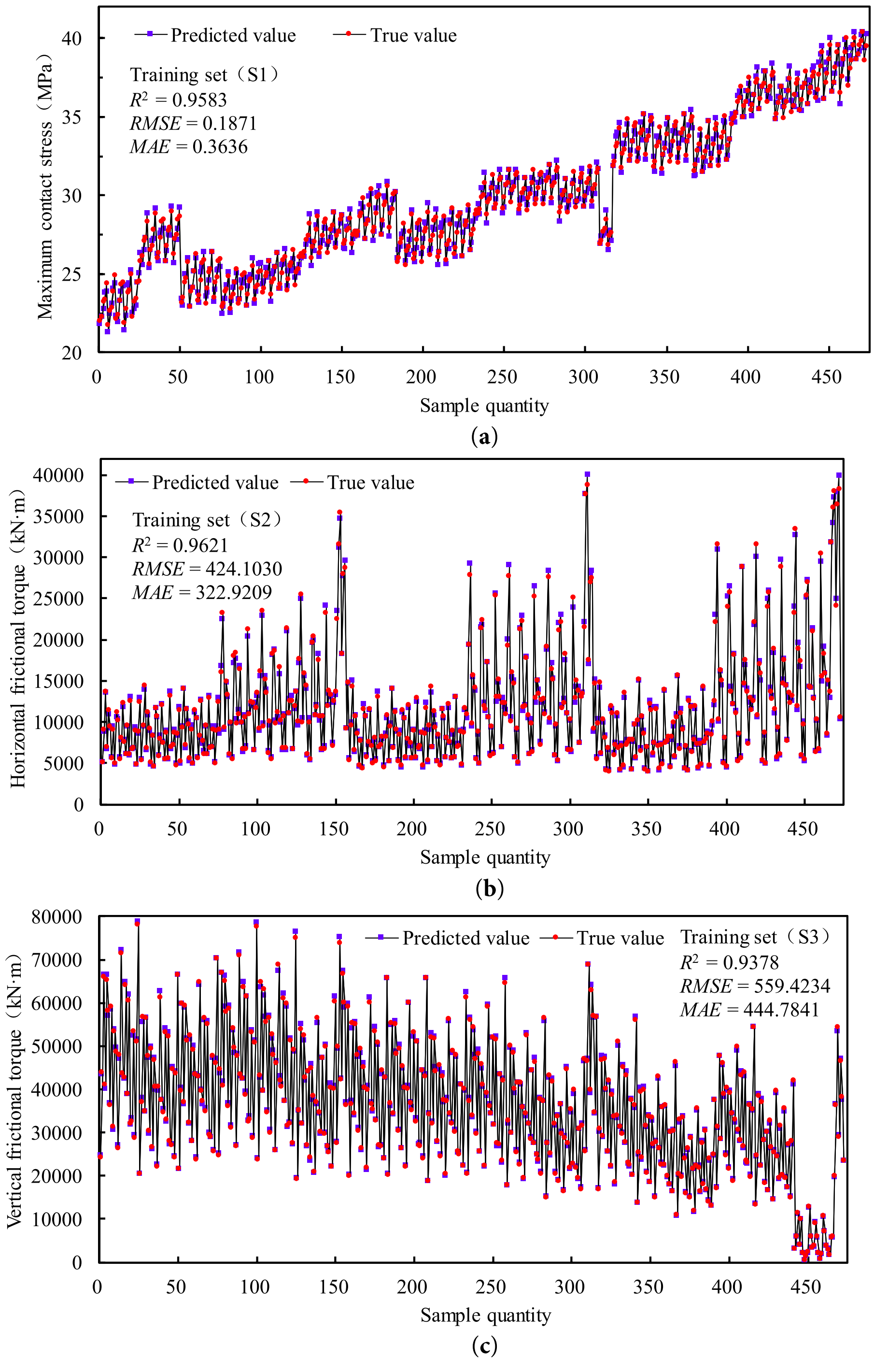

Figure 11: Fit of SVR metamodel training set. (**a**) S1 Training set; (**b**) S2 Training set; (**c**) S3 Training set.

5 Parametric Sensitivity Analysis of Ball-Hinge Force Characteristics

Related studies have shown [21–26] that the results of the sensitivity analysis may vary depending on the training samples, so in this study the parametric sensitivity analysis of the force characteristics of the ball-hinge contact surfaces was carried out using Morris's basic effects method and Sobol's exponential model with different sample sizes.

The results of the sensitivity analysis are affected by the sampling accuracy. Seven input parameters are considered in the sample data of this study, of which three input parameters (X1, X2, X3) are set to three levels, while the remaining four parameters (X4, X5, X6, X7) are set to five levels, and the full permutation of which can be up to $3^3 \times 5^4 = 16{,}875$ groups of working conditions. Considering the computational efficiency and cost, this paper numerically calculates 675 sets of working conditions, and applies the SVR metamodel of ball-hinge contact surface force characteristics constructed above instead of numerical calculation, and expands the data set of these 675 sets of working conditions to 16,875 sets of fully-aligned working conditions, in order to satisfy the requirements of the number of sampling samples and sampling accuracy in the process of sensitivity analysis.

5.1 Latin Hypercube Sampling

Sampling methods for parametric sensitivity analysis include Sobol sequence sampling, Monte Carlo sampling and other methods [23], the most commonly used is the Monte Carlo method based on Latin hypercubic sampling. Latin hypercubic sampling can obtain higher accuracy with smaller sampling size, and can also improve the distribution space of sampled values, showing better performance and efficiency in practical applications.

The basic principle of Latin hypercube sampling is to divide each dimension coordinate interval ($[x_{kmin}, x_{kmax}]$, i ∈ $[1, n]$) into m sub-intervals in n-dimensional space, and to draw a $m \times$ n group of sample points in each sub-interval ($[x_k^{i-1}, x_k^i]$, i ∈ $[1, m]$). However, this method fails to consider the uniformity of the distribution between the sample points, and has defects in the calculation accuracy, and cannot realize the "uniform space filling" of the sample points.

Therefore, in this paper Latin Hypercube Sampling is improved by using Maximum Minimum Distance method $[a_1, b_1]$ to get the optimized Latin Hypercube Sampling method, which maximizes the minimum distance between the sample points, in order to increase the dispersion and uniformity between the sample points. Taking 100 sampled data points in two-dimensional space as an example, Fig. 12 shows the comparison of the sampling effect of the Latin hypercube sampling method before and after optimization. It can be found that the optimized Latin Hypercube sampling has better uniformity and randomness in the distance between each sample point, and the sampling is more uniform.

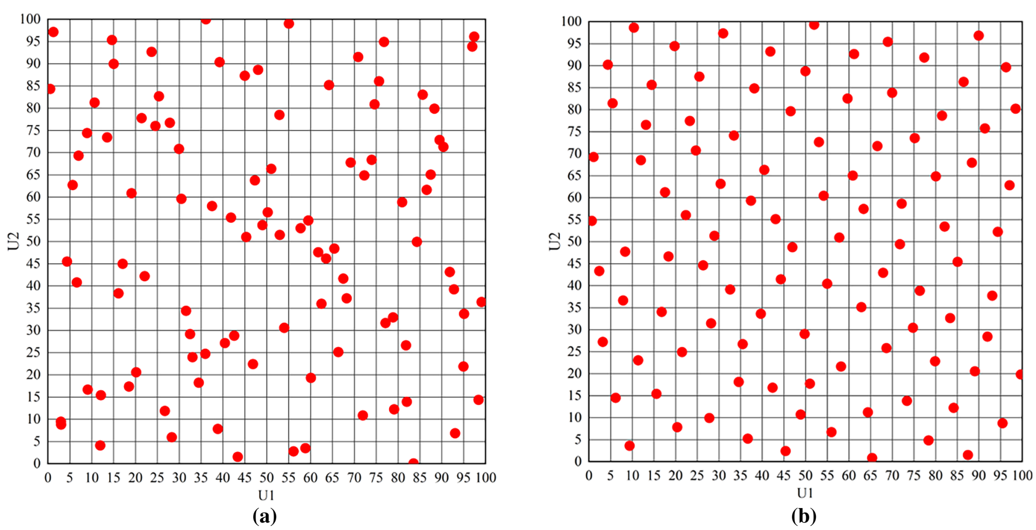

Figure 12: Sampling effect of Latin hypercube sampling method before and after optimization. (**a**) Latin hypercube sampling; (**b**) Optimized Latin hypercube sampling.

In this study, 16,875 groups of working conditions after the expansion of SVR model prediction are used as the sample database, and the optimized Latin superlattice method is applied for sampling, and the number of samples is set to 500, 1000, 2000, 4000, 8000, and 16,000 in total 6 cases, which is used as the data base for sensitivity analysis.

5.2 Parameter Sensitivity Analysis

(1) Morris Basic Effects Approach

The Morris basic effects approach, commonly used for estimating sensitivity measures, involves using an efficient sampling design to cover a set of sampling trajectories in an uncertain input domain [27,28]. For a model containing m variables, multiple initial vectors of variables are randomly generated, and the basic effects index for the ith input variable is calculated separately as:

$$d_i^*\left(\boldsymbol{x}\right) = \left|\frac{M^*\left(\boldsymbol{x}\right) - M\left(\boldsymbol{x}\right)}{\Delta}\right| \tag{8}$$

In the above equation, $d_i^*\left(\boldsymbol{x}\right)$is the basic effect index;

notation$M\left(\boldsymbol{x}\right) = M\left(x_1, x_2, \cdots, x_i, x_{i+1}, \cdots, x_M\right)$, denotes the objective function;

$M^*\left(\boldsymbol{x}\right) = M\left(x_1, x_2, \cdots, x_i + \Delta, x_{i+1}, \cdots, x_M\right)$, denotes the objective function after parameter change; Δ is the amount of parameter x_i change.

In this study, the corrected mean $\mu_i{}^*$ and standard deviation σ_i were used to determine the sensitivity of each parameter:

$$\mu_i^* = \frac{1}{t}\sum\nolimits_{j=1}^{t}\left|d_i\left(j\right)\right| \tag{9}$$

$$\sigma_i = \sqrt{\frac{1}{t-1}\sum\nolimits_{j=1}^{t}\left|d_i\left(j\right) - \mu_i{}^*\right|^2} \tag{10}$$

where $d_i(j)$ denotes the base effect of the *jth* set of samples for the *ith* parameter; $j = 1, 2, \ldots, t$ (where t is the number of repeated samples). $\mu_i{}^*$ characterizes the significance of the effect of the input variables on the output of the model, which is positively correlated. σ is used as a measure of nonlinearity of the input variables on the model and interactions among variables, which are also positively correlated, and such nonlinearity and interactions have important implications for the complexity and predictive power of the model.

In the parametric sensitivity analysis of the force characteristics of the bridge's rotating ball hinge, the Morris basic effect method was used to identify the degree of influence of the input parameters X1 to X7 on the output parameters S1 to S3, and the specific results are shown in Tables 8–10. It can be found that the sensitivity analysis results of the Morris method are not consistent under different sample sizes, and the rankings of μ and σ change with different sample sizes.

When the sample size increases from 1000 to 16,000, the distribution of the maximum μ values is as follows: For S1, the inputs are X2, X5, X2, X7, X7, X7 in sequence; for S2, the inputs are X1, X1, X6, X6, X6, X6; and for S3, the inputs are X7, X6, X6, X7, X7, X7. As for the distribution of the maximum σ values: For S1, they are X7, X4, X4, X2, X7, X7; for S2, they are X1, X6, X7, X6, X6, X6; and for S3, they are X2, X7, X2, X2, X7, X7.

Table 8: Sensitivity analysis results of Morris basic effects method for 10 S1 (maximum contact stress).

Sample Size	Evaluation Indicators	X1	X2	X3	X4	X5	X6	X7
1000	μ*	0.2255	0.2821	0.2056	0.1043	0.2922	0.0504	0.2867
	σ	0.0022	0.0027	0.0015	0.0029	0.0007	0.0008	0.0028
4000	μ*	0.2472	0.2969	0.2099	0.1120	0.2309	0.0526	0.3186
	σ	0.0023	0.0028	0.0015	0.0029	0.0007	0.0009	0.0027
16,000	μ*	0.2550	0.3124	0.2186	0.1067	0.2357	0.0531	0.3321
	σ	0.0024	0.0028	0.0016	0.0027	0.0007	0.0008	0.0032

Table 9: Sensitivity analysis results of Morris's basic effects method for S2 (horizontal moment of resistance).

Sample Size	Evaluation Indicators	X1	X2	X3	X4	X5	X6	X7
1000	μ*	0.4251	0.2423	0.2988	0.1053	0.1660	0.3447	0.3647
	σ	0.0763	0.0384	0.0703	0.0526	0.0717	0.0866	0.0666
4000	μ*	0.4007	0.2450	0.2845	0.1035	0.1782	0.4435	0.3439
	σ	0.0734	0.0392	0.0698	0.0496	0.0703	0.0721	0.0701
16,000	μ*	0.3780	0.2381	0.2735	0.0957	0.1748	0.4349	0.3338
	σ	0.0741	0.0377	0.0639	0.0496	0.0740	0.0877	0.0648

Table 10: Sensitivity analysis results of the Morris basic effects method for 12 S3 (vertical moment of resistance).

Sample Size	Evaluation Indicators	X1	X2	X3	X4	X5	X6	X7
1000	μ*	0.1954	0.2963	0.5674	0.1282	0.2229	0.0396	0.6569
	σ	0.0878	0.0512	0.0651	0.0830	0.0873	0.1164	0.0681
4000	μ*	0.0476	0.4776	0.4366	0.7357	0.5033	0.0464	0.2664
	σ	0.0240	0.0503	0.0299	0.0733	0.0675	0.0473	0.0908
16,000	μ*	0.2165	0.5115	0.3357	0.7395	0.0514	0.5009	0.2081
	σ	0.0766	0.1068	0.0747	0.0261	0.0259	0.0473	0.0957

When the number of samples in the training set for S1, S2 and S3 is greater than 4000, then the sensitivity analysis results become stable and can be analyzed and inferred by μ and σ. The results show that the sensitivity analysis results using the Morris method are not stable, and the sensitivity analysis results become stable only when the sample size exceeds a certain value, which can be set to 4000 in this study.

The sensitivity results when the number of samples is 16,000 times are shown in Fig. 13, by analyzing the graphical results, the sensitivity of different input parameters to each output parameter is different. For the characteristic index S1 (maximum contact stress), the indexes with significant influence on it are X7, X2, X1 in order, for the characteristic index S2 (horizontal moment of resistance), the indexes with significant influence on it are X6, X1, X7 in order, and for the characteristic index S3 (vertical moment of resistance), the indexes with significant influence on it are X7, X6, X2 in order, which indicates that special attention should be paid to these parameters in the design and optimization process to ensure the safety and stability of the structure. these parameters to ensure the safety and stability of the structure.

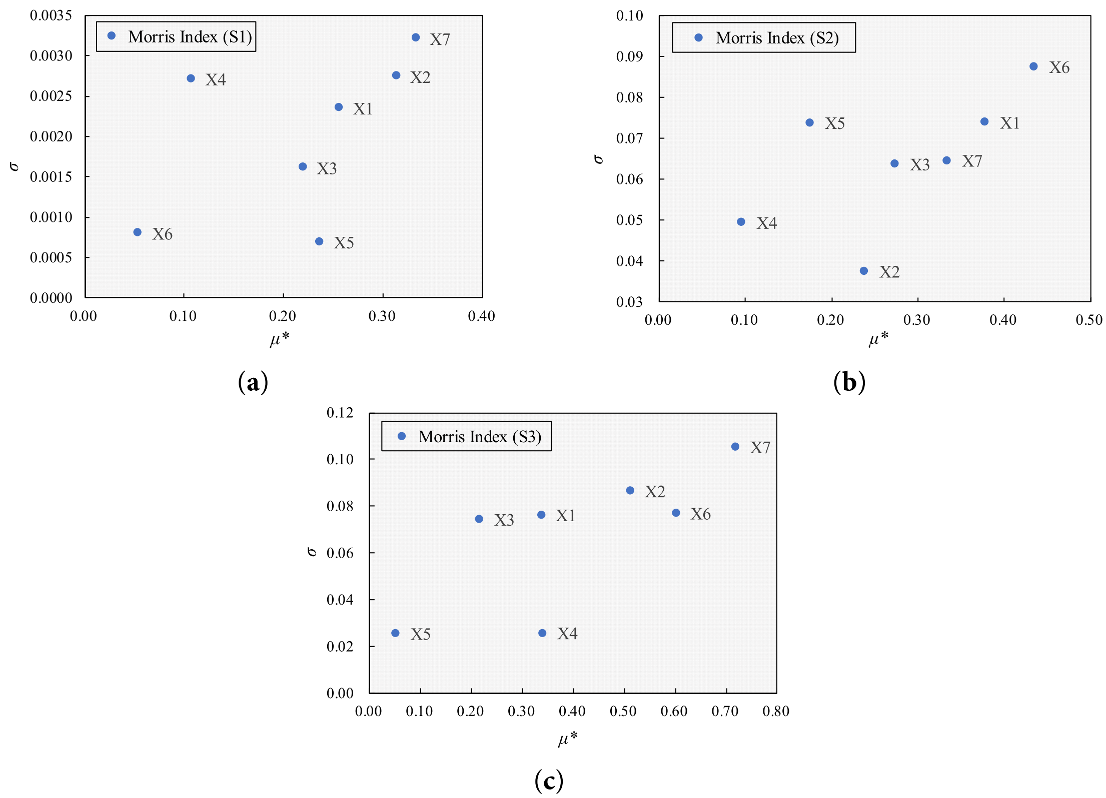

Figure 13: Morris index for 13-parameter sensitivity analysis. (**a**) Characterization indicator S1; (**b**) Characterization indicator S2; (**c**) Characterization indicator S3.

(2) Sobol exponential modeling method

The Sobol model is an analytical method based on multiple integrals [29,30], and in applying the Sobol model for sensitivity analysis, it is necessary to define the domain of the set of input parameters, Ω^k, i.e.,

$$\Omega^k = \{x \,|0 \le x_i \le 1, i = 1, 2, \cdots, k\} \tag{11}$$

In the above equation, Ω^k is the cell body; $_{x(i)}$ is the covariate, i.e., the input variable; and k is the dimension, i.e., the number of input variables.

For the objective function $f(x)$, both can be expressed in the form of a sum of 2^k subterms, i.e.,

$$f\,(x) = f_0 + \sum_{i=1}^{k} f_i\,(x_i) + \sum_{1 \le i < j \le k} f_{ij}\left(x_i, x_j\right) + \cdots + f_{1,2,\cdots,k}\,(x_1, x_2, \cdots, x_k) \tag{12}$$

The total variance D of the model objective function $f(x)$ is:

$$D = \int_{\Omega^k} f^2\,(x)\,dx - f_0^2 = \sum_{s=1}^{k} D_i + \sum_{1 \le i < j \le k} D_{ij} + D_{1,2,\cdots,k} \tag{13}$$

In the above equation, it can be found that the total variance of the function is equal to the sum of the variances of its subsections, and the variances of the subsections are the partial variances of each order, and the s-order variance can be expressed as:

$$D_{i_1,i_2,\cdots,i_s} = \int_0^1 \cdots \int_0^1 f^2_{i_1,i_2,\cdots,i_s}(x_{i_1}, x_{i_2}, \cdots, x_{i_s})\, dx_{i_1} dx_{i_2} \cdots dx_{i_s} \tag{14}$$

The evaluation indicators of the Sobol model include the main effects sensitivity index MSI_i and the total effects sensitivity index $TSI_{(i)}$:

$$MSI_i = \frac{D_i}{\sum_{i=1}^{k} D_i + \sum_{1 \le i < j \le k} D_{ij} + \ldots + D_{1,2,\cdots,k}} \tag{15}$$

$$TSI_i = 1 - \frac{D_{\sim i}}{\sum_{i=1}^{k} D_i + \sum_{1 \le i < j \le k} D_{ij} + \ldots + D_{1,2,\cdots,k}} \tag{16}$$

In the above equation, MSI_i and TSI_i represent the main effect sensitivity index and total effect sensitivity index, respectively; D_i, D_{ij}, $D_{1,2,...,k}$ denote the *1st*-order, *2nd*-order, and *kth*-order variances, respectively; $D_{\sim i}$ represents the variance under the joint influence of variables other than x_i; and k is the number of variables.

In this study, the Sobol index method was used to identify the degree of influence of input parameters X1 to X7 on output parameters S1 to S3 as shown in Tables 11–13.

Table 11: Sobol method sensitivity analysis results for S1 (maximum contact stress).

Sample Size	Evaluation Indicators	X1	X2	X3	X4	X5	X6	X7
500	MSI	0.3106	0.2408	0.0131	0.0247	0.0153	0.0234	0.3721
	TSI	0.3231	0.2439	0.0247	0.0012	0.0113	0.0156	0.3802
1000	MSI	0.3137	0.2317	0.0214	0.0262	0.0053	0.0222	0.3795
	TSI	0.2891	0.2744	0.0153	0.0012	0.0149	0.0160	0.3891
2000	MSI	0.3263	0.2302	0.0129	0.0425	0.0004	0.0233	0.3644
	TSI	0.3122	0.2479	0.0269	0.0022	0.0202	0.0276	0.3631
4000	MSI	0.3295	0.2114	0.0314	0.0239	0.0025	0.0224	0.3789
	TSI	0.3163	0.2273	0.0345	0.0021	0.0207	0.0268	0.3723
8000	MSI	0.3460	0.1915	0.0214	0.0425	0.0134	0.0215	0.3638
	TSI	0.3154	0.2289	0.0266	0.0025	0.0223	0.0293	0.3750
16,000	MSI	0.3261	0.2112	0.0213	0.0326	0.0045	0.0228	0.3815
	TSI	0.3097	0.2497	0.0338	0.0025	0.0227	0.0271	0.3544

Table 12: Sobol method sensitivity analysis results for S2 (horizontal moment of friction).

Sample Size	Evaluation Indicators	X1	X2	X3	X4	X5	X6	X7
500	MSI	0.3861	0.0319	0.0142	0.0059	0.0152	0.3006	0.2461
	TSI	0.4023	0.0204	0.0039	0.0105	0.0087	0.2811	0.2931
1000	MSI	0.3848	0.0339	0.0144	0.0057	0.0169	0.2951	0.2492
	TSI	0.4093	0.0195	0.0037	0.0104	0.0083	0.2813	0.2575

(Continued)

Table 12 (continued)

Sample Size	Evaluation Indicators	X1	X2	X3	X4	X5	X6	X7
2000	MSI	0.3804	0.0459	0.0152	0.0062	0.0178	0.2857	0.2488
	TSI	0.3953	0.0222	0.0035	0.0099	0.0081	0.2956	0.2589
4000	MSI	0.3708	0.0333	0.0222	0.0170	0.0224	0.2672	0.2673
	TSI	0.4202	0.0185	0.0033	0.0160	0.0089	0.2933	0.2469
8000	MSI	0.3640	0.0521	0.0157	0.0065	0.0193	0.2674	0.2751
	TSI	0.4137	0.0232	0.0039	0.0101	0.0080	0.2717	0.2754
16,000	MSI	0.3678	0.0329	0.0168	0.0067	0.0219	0.2911	0.2628
	TSI	0.4205	0.0242	0.0038	0.0169	0.0092	0.2965	0.2448

Table 13: Sobol method sensitivity analysis results for S3 (vertical moment of resistance).

Sample Size	Evaluation Indicators	X1	X2	X3	X4	X5	X6	X7
500	MSI	0.3535	0.1848	0.0222	0.0186	0.0042	0.2123	0.2031
	TSI	0.3622	0.1753	0.0262	0.0159	0.0039	0.2045	0.1792
1000	MSI	0.3747	0.1719	0.0283	0.0156	0.0064	0.2208	0.1889
	TSI	0.3782	0.1903	0.0204	0.0164	0.0039	0.1974	0.2092
2000	MSI	0.3710	0.1770	0.0389	0.0262	0.0044	0.2186	0.1757
	TSI	0.3556	0.1827	0.0262	0.0177	0.0039	0.1856	0.2092
4000	MSI	0.3784	0.1646	0.0339	0.0160	0.0074	0.2055	0.1862
	TSI	0.3804	0.1827	0.0272	0.0248	0.0041	0.1726	0.2050
8000	MSI	0.3557	0.1613	0.0323	0.0215	0.0086	0.2157	0.1881
	TSI	0.3919	0.1864	0.0313	0.0222	0.0074	0.1709	0.1927
16,000	MSI	0.3841	0.1662	0.0379	0.0339	0.0084	0.2114	0.2012
	TSI	0.4093	0.1994	0.0323	0.0219	0.0076	0.1743	0.1889

Fig. 14. shows the distribution of Sobol index for parameter sensitivity analysis, from the Fig. 13, the TSI and MSI indices for the three characteristic indicators show good consistency for the same input indexes, which also influences the factors, whether in the univariate case or multivariate combined role, the impact on the output results are at a relatively similar level, for S1, the more influential For S1, the more influential input variables are X7, X1, and X2; for S2, the more influential input variables are X1, X6, and X7; and for S3, the more influential input variables are X1, X6, X7, and X2, which is in good agreement with the results of the Morris Index sensitivity analysis mentioned above.

When the number of samples is greater than 4000, for S1~S3, then the rankings of MSI and TSI on sensitive input parameters are stable. By comparing the results of the sensitivity analyses of MSI and TSI, it is found that the rankings of the input variables with higher sensitivity do not show significant changes, which indicates that the interaction effects of the input parameters have less influence on the output results. As the sample size increases, X7, X1 and X1 are always the most sensitive parameters corresponding to S1, S2 and S3, respectively. It is also found that the sensitivity analysis results of the Sobol method become stable after the sample size exceeds a certain value, which can be set to 4000 in this study.

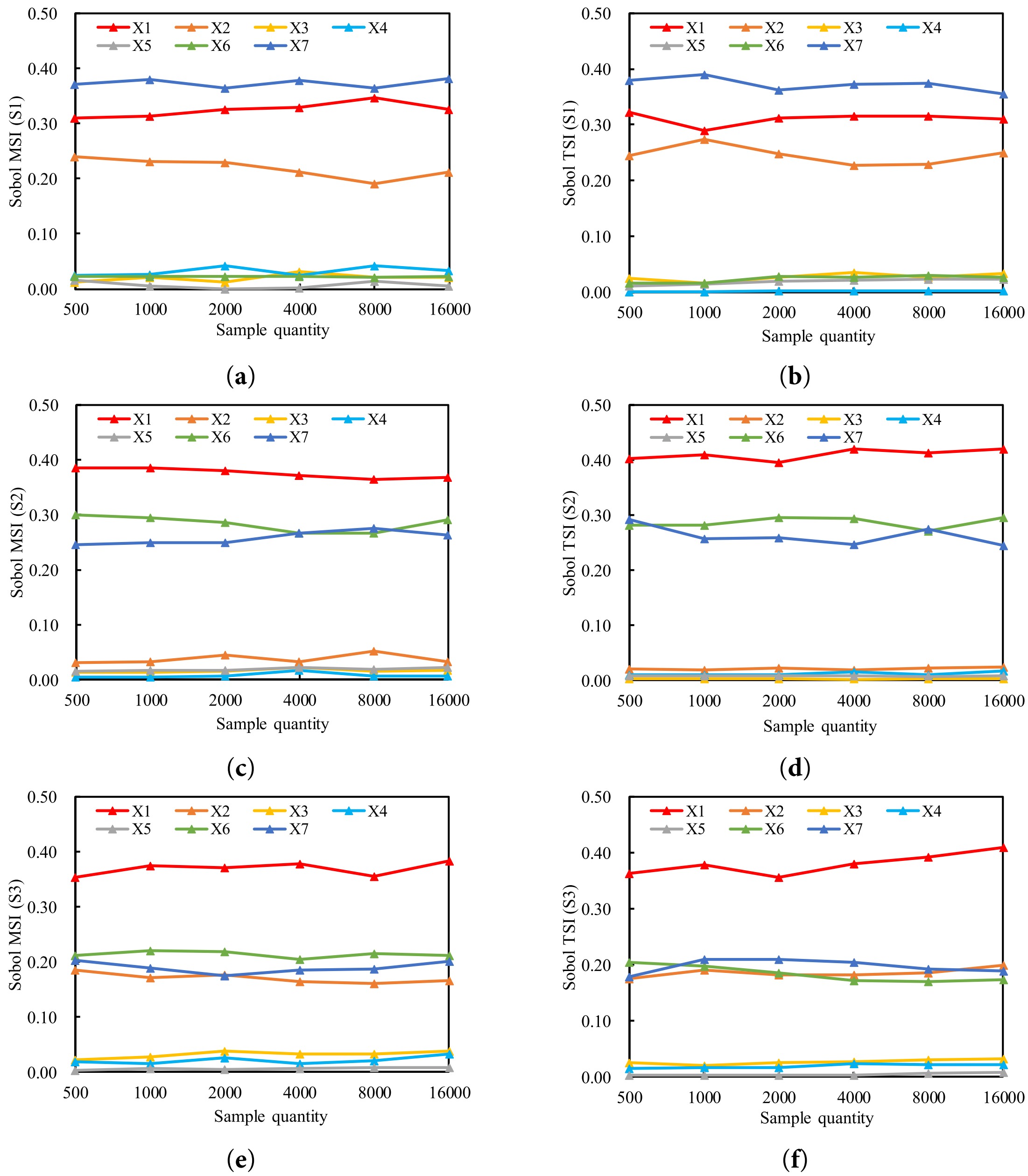

Figure 14: Sobol index for 14-parameter sensitivity analysis. (**a**) Sobol MSI (S1); (**b**) Sobol TSI (S1); (**c**) Sobol MSI (S2); (**d**) Sobol TSI (S2); (**e**) Sobol MSI (S3); (**f**) Sobol TSI (S3).

Parameter sensitivity analysis reveals that increasing the bearing radius significantly reduces the maximum contact stress of the ball joint, while the rotational weight leads to a linear increase in stress, with both factors jointly determining the stress distribution. Simultaneously, reducing the curvature radius and increasing the friction coefficient substantially enhance the horizontal and vertical friction torque of the ball joint, with the rotational weight amplifying this effect. The bearing radius and rotational weight influence the maximum contact stress of the ball joint in opposing directions by altering the contact area and load distribution, respectively. Meanwhile, the curvature radius, friction coefficient, and rotational weight synergistically affect the friction torque, with the friction coefficient demonstrating the highest sensitivity to torque.

In summary, the Sobol indices of the constituents calculated using the data from the ABAQUS finite element simulation are in good agreement with the nature of the actual force characteristics of the ball-and-hinge structure. It is also shown that the finite element simulation calculations and the elemental model proposed in this study can map the force characteristics of the ball-hinged structure in the actual situation to a certain extent.

6 Design and Maintenance Recommendations

Based on the sensitivity analysis results, the following recommendations are proposed for the design and maintenance of spherical hinges in swing bridges:

(1) Increasing the support radius significantly reduces maximum contact stress. It is recommended to adopt a support radius of at least 2200 mm for bridges with swing weights exceeding 16,000 t to ensure stress levels remain within safe limits.
(2) A smaller curvature radius increases frictional moments, which may hinder smooth rotation. A curvature radius between 9000 and 10,000 mm is recommended to balance frictional resistance and structural stability.
(3) The friction coefficient exhibits high sensitivity to both horizontal and vertical frictional moments. Regular lubrication and anti-corrosion treatments are essential to maintain a friction coefficient below 0.05, ensuring smooth rotation and reducing wear.
(4) The swing weight directly influences contact stress and frictional moments. Accurate weight estimation during construction is critical, and any deviation should be compensated by adjusting other design parameters.
(5) It is recommended to periodically measure the friction coefficient and contact surface condition using non-destructive techniques to detect early signs of wear or lubrication failure.

7 Conclusions and Prospects

This study systematically investigates the contact friction behavior of spherical hinges in swing bridges using finite element modeling and metamodel-based sensitivity analysis. A refined FE model of an actual swing bridge was established, and an SVR-based metamodel was developed to efficiently predict maximum contact stress, horizontal frictional moment, and vertical frictional moment. Compared with conventional parametric analysis, the proposed framework significantly improves computational efficiency while maintaining high accuracy, enabling comprehensive multi-parameter sensitivity evaluation. The main conclusions are as follows:

(1) A metamodel of the contact friction characteristics of the ball hinge was constructed based on three methods, namely, PCE, Kriging and SVR, with seven parameters of the ball hinge, namely, radius of curvature, radius of support, radius of pinning, modulus of elasticity, Poisson's ratio, coefficient of friction, and weight of the rotating body, as the input indexes, and three variables of the maximum contact stress, vertical moment of friction, and horizontal moment of friction as the output indexes (characteristics). The prediction accuracy and fitting indexes of the three methods are compared and analyzed, and the applicability and reliability of the proposed metamodel in the simulation of the mechanical behavior of the ball hinge are evaluated, which provides an effective numerical tool for the rapid prediction of the contact friction characteristics of the ball hinge.
(2) Through comparative analysis, it is found that when the sample size is 500~600, the metamodel established by using SVR has a better generalization ability and fitting effect for the sample data of this study. The $R^2_{adjusted}$ mean values of the three feature indicators S1~S3 under 50 times of resampling can

reach 0.9593, 0.9557, 0.9429, and the maximum values can reach 0.9941, 0.9925, respectively, 0.9967, which has a good ability to explain and generalize the sample data.

(3) The results of the sensitivity analysis show that for the variable factors with the greatest influence on each characteristic index, the results of the Morris basic effect method and the Sobol index model method are in good agreement. For the maximum contact stress, the more influential factors are the support radius and the weight of the rotating body in order; for the vertical moment of friction and the horizontal moment of friction, the more influential factors are the radius of curvature, the friction coefficient and the weight of the rotating body in order. It is also found that the results of parameter sensitivity analysis in this study become stable when the sample size exceeds 4000.

Further research will focus on experimental validation of the proposed metamodel using scaled or full-scale spherical hinge specimens. Additionally, the integration of time-dependent material behavior and temperature effects into the metamodel framework will be explored to enhance its applicability under varying environmental conditions.

Optimization and Calibration of a Mechanical Analytical Model for Contact Stresses in Rotating Spherical Hinge Joints. In the future, by combining the strengths of metamodels with those of mechanical analytical models, it will be possible to achieve more refined model calibration and optimization, thereby providing more accurate and reliable theoretical support for the design and analysis of rotating bridge spherical hinge joints.

Acknowledgement: Not applicable.

Funding Statement: The authors would like to acknowledge the financial support received from Science Foundation Project for Outstanding Youth of Henan Province (Grant No.232300421014) and the key scientific research projects of colleges and universities in Henan Province (Grant No.23ZX014), as well as the National Natural Science Foundation of China (Grant No.52279144/523791374).

Author Contributions: Writing—original draft and software, Jiahao Wang; methodology and funding acquisition, Yuanxun Zheng; resources and supervision, Chaowei Du; supervision and visualization, Shuaijie Zhang; software and data curation, Xiangyang Chen; project administration, Xiaojun Che; formal analysis, Fuhua Wang. All authors reviewed and approved the final version of the manuscript.

Availability of Data and Materials: Not applicable.

Ethics Approval: Not applicable.

Conflicts of Interest: The authors declare no conflicts of interest.

Abbreviations

PC	Prestressed Concrete
SVR	Support Vector Regression
PCE	Polynomial Chaos Expansion
RBF	Radial Basis Function
SVMs	Support Vector Machines

Appendix A

List of symbols.

Symbol	Description
σ	Contact stress (MPa)

r	Distance from spherical hinge center (mm)
A, B, C, D	Fitting coefficients
R^2	Coefficient of determination
μ^*	Morris sensitivity index
σ_i	Morris standard deviation
MSI	Main effect sensitivity index
TSI	Total effect sensitivity index

References

1. Bonopera M, De Matteis G. Analysis of the shear deformation in simply supported prestressed concrete girder-bridges. Procedia Struct Integr. 2026;78(14):1143–50. doi:10.1016/j.prostr.2025.12.146.
2. Parsons B, Wilson EA. A method for determining the surface contact stresses resulting from interference fits. J Eng Ind. 1970;92(1):208–18. doi:10.1115/1.3427710.
3. Chan SK, Tuba IS. A finite element method for contact problems of solid bodies: part I. Theory and Validation. Int J Mech Sci. 1971;13(7):615–25. doi:10.1016/0020-7403(71)90032-4.
4. Wang JQ, Bryant DM, Keer ML, Salant RF. Virtual tribology: integrating model-based simulations with modern computation/information technologies. Comput Model Eng Sci. 2002;3(4):417–30. doi:10.3970/cmes.2002.003.417.
5. Liu S, Liu J, Huang Y, Zheng Y. Optimization of swivel spherical hinge structure design based on the response surface method. Sustainability. 2023;15(13):10356. doi:10.3390/su151310356.
6. He S. A study on contact analysis and equilibrium control of spherical joints in the construction of rotating-to-fixed joints [dissertation]. Chongqing, China: Chongqing Jiaotong University. 2021. (In Chinese). doi:10.27671/d.cnki.gcjtc.2021.000104.
7. Sun Z, Hao C. Conformal contact problems of ball-socket and ball. Phys Procedia. 2012;25(1):209–14. doi:10.1016/j.phpro.2012.03.073.
8. Huang S, Hu M, Huang Y, Cui N, Wang W. A new model for optimal mechanical and thermal performance of cement-based partition wall. Materials. 2018;11(4):615. doi:10.3390/ma11040615.
9. Jiang L, Gao R. Deformation monitoring during removal of the supporting of T-type rigid frame bridge constructed by rotation method. Procedia Eng. 2010;4(2):355–60. doi:10.1016/j.proeng.2010.08.041.
10. Fang X. Coordinated contact modeling and wear life prediction for joint bearings [dissertation]. Changsha, China: National University of Defense Technology; 2014. (In Chinese).
11. Shi X, Liu Z, Guo T, Cai CS, Jiang C. Investigation on contact stress calculation method of spherical hinge structures for swivel construction. Structures. 2024;69:107290. doi:10.1016/j.istruc.2024.107290.
12. Lan Y. Mechanical analysis and application research of horizontal swivel spherical joint [dissertation]. Shijiazhuang, China: Shijiazhuang Railway University; 2018. (In Chinese).
13. Ye J, Zhou H, Peng H, Bu Z, Xu S. Transverse vehicle distribution coefficient study of small box girder bridges with obvious or hidden bent cap. J Phys Conf Ser. 2025;3027(1):012083. doi:10.1088/1742-6596/3027/1/012083.
14. Liang J, Lei S, Li K. Optimization calculation method and weighing test of static friction coefficient of RPC spherical joint based on half space contact model. IOP Conf Ser Earth Environ Sci. 2020;446(5):052034. doi:10.1088/1755-1315/446/5/052034.
15. Rodríguez-Romero R, Compán V, Sáez A, García-Macías E. Hierarchical meta-modelling for fast prediction of the elastic properties of stone injected with CNT/cement mortar. Constr Build Mater. 2023;408(8):133725. doi:10.1016/j.conbuildmat.2023.133725.
16. Murcia JP, Réthoré PE, Dimitrov N, Natarajan A, Sørensen JD, Graf P, et al. Uncertainty propagation through an aeroelastic wind turbine model using polynomial surrogates. Renew Energy. 2018;119(2):910–22. doi:10.1016/j.renene.2017.07.070.
17. Zheng X, Yao W, Gong Z, Zhang X. Learnable quantile polynomial chaos expansion: an uncertainty quantification method for interval reliability analysis. Reliab Eng Syst Saf. 2024;245(6):110036. doi:10.1016/j.ress.2024.110036.

18. Palar PS, Zuhal LR, Shimoyama K, Tsuchiya T. Global sensitivity analysis via multi-fidelity polynomial chaos expansion. Reliab Eng Syst Saf. 2018;170(1):175–90. doi:10.1016/j.ress.2017.10.013.
19. Appriou T, Rullière D, Gaudrie D. Combination of optimization-free Kriging models for high-dimensional problems. Comput Stat. 2024;39(6):3049–71. doi:10.1007/s00180-023-01424-7.
20. Vapnik VN. The nature of statistical learning theory. New York, NY, USA: Springer New York; 1995. doi:10.1007/978-1-4757-2440-0.
21. Zheng J, Shao X, Gao L, Jiang P, Li Z. A hybrid variable-fidelity global approximation modelling method combining tuned radial basis function base and Kriging correction. J Eng Des. 2013;24(8):604–22. doi:10.1080/09544828.2013.788135.
22. Gan Y, Duan Q, Gong W, Tong C, Sun Y, Chu W, et al. A comprehensive evaluation of various sensitivity analysis methods: a case study with a hydrological model. Environ Model Softw. 2014;51(1–2):269–85. doi:10.1016/j.envsoft.2013.09.031.
23. Jia H, Xu T, Liang S, Zhao P, Xu C. Bayesian framework of parameter sensitivity, uncertainty, and identifiability analysis in complex water quality models. Environ Model Softw. 2018;104(3):13–26. doi:10.1016/j.envsoft.2018.03.001.
24. Saxton H, Xu X, Schenkel T, Clayton RH, Halliday I. Convergence, sampling and total order estimator effects on parameter orthogonality in global sensitivity analysis. PLoS Comput Biol. 2024;20(7):e1011946. doi:10.1371/journal.pcbi.1011946.
25. Guo W, Yu H, Li Y, Tian W, Chen W. Mechanical characteristics and design parameter analysis of spherical hinge structure for swivel bridge. Sci Rep. 2024;14(1):29922. doi:10.1038/s41598-024-81320-2.
26. Bai X, Zeng J, Chen KS, Li Z, Zeng Y, Wen J, et al. Parameter optimization of a discrete scattering model by integration of global sensitivity analysis using SMAP active and passive observations. IEEE Trans Geosci Remote Sens. 2019;57(2):1084–99. doi:10.1109/TGRS.2018.2864689.
27. Morris MD. Factorial sampling plans for preliminary computational experiments. Technometrics. 1991;33(2):161–74. doi:10.1080/00401706.1991.10484804.
28. Campolongo F, Cariboni J, Saltelli A. An effective screening design for sensitivity analysis of large models. Environ Model Softw. 2007;22(10):1509–18. doi:10.1016/j.envsoft.2006.10.004.
29. Sobol IM. Monte Carlo estimates. Math Comput Simul. 2001;55(1–3):271–80. doi:10.1016/S0378-4754(00)00270-6.
30. Todorov V, Stoenchev M. Advanced stochastic methods for estimating sensitivity indices. In: AIP Conference Proceedings. Dhi-Qar, Iraq: AIP Publishing; 2025. doi:10.1063/5.0247256.